Materials Advances

ROYAL SOCIETY OF CHEMISTRY

PAPER

View Article Online
View Journal | View Issue

Cite this: *Mater. Adv.*, 2021, **2**, 2626

Non-toxic layered double hydroxide nanoplatelet dispersions for gas barrier coatings on flexible packaging†

Kanittika Ruengkajorn, Chunping Chen, Jingfang Yu, Jean-Charles Buffet and Dermot O'Hare *

Received 16th December 2020,
Accepted 1st March 2021

DOI: 10.1039/d0ma00986e

rsc.li/materials-advances

High gas barrier, transparent and non-toxic coatings are in increasing demand due to the need to develop easier recyclable food packaging technologies. Herein, we report a green synthesis of layered double hydroxide (LDH) nanoplatelets *via* a reconstruction process in concentrated amino acid solution. The effect of both the amino acid (nonpolar and polar) and the original LDH morphology (rosette and large platelet) on the formation of uniform dispersed LDH nanoplatelets was systematically studied. LDH nanosheet dispersions in polyvinyl alcohol (PVA) were coated on polyethylene terephthalate (PET) substrates. The oxygen barrier performance and optical properties of the LDH nanosheet coated PET films were evaluated. We found that the PET coated films retained excellent optical responses and exhibited a high oxygen barrier, with an oxygen transmission rate down to 0.35 cc m^{-2} day^{-1}. This represents an oxygen barrier improvement factor (BIF) between the coated and uncoated PET films of 175.

Introduction

The demand for the development of flexible, transparent and recyclable packaging materials has increased in many sectors such as in food and beverages, cosmetics, healthcare, and electronics.[1–3] The incorporation of impermeable inorganic platelet fillers can improve the gas-barrier properties of polymers by increasing the diffusion pathway of the permeating molecules, generally referred to as a tortuous pathway.[4–6] However, the non-uniform particle size, random alignment, aggregation, and phase separation of such platelets can drastically decrease the barrier performance.[7,8] Although, nanostructured artificial nacre-like clay-based materials have been reported, they are not highly transparent due to their high loading of fillers and thick coating layers.[8–10] Therefore, there is urgent need for the development of well dispersed, uniform and thin inorganic nanosheets to obtain high gas barrier films with good transparency. The exfoliation/delamination of layered materials (graphite and graphite-like materials,[11–16] metal oxides,[17,18] zirconium phosphate[19,20] and clays[21,22]) has attracted the most attention so far since these materials can yield thin nanosheets with a high aspect ratio.[23–28] A wide variety of exfoliation methods have been developed, such as sonication/high shear mixing in surfactants,[11,12,14] solvents,[13,15,19] and polymers.[12,17,22] Pre-modification by ion exchange with spatially demanding molecules to produce large interlayer separations followed by exfoliation has been extensively explored.[16,18,20,22] Although, the use of layered silicate materials has been widely reported, they can only be exchanged with a limited range of cations, mostly alkyl-ammonium based, which restricts their modification and potential applications.[23]

Layered double hydroxides (LDHs) are a large family of 2D layer materials which consist of a positively charged brucite-like layer and a negatively charged interlayer with exchangeable anions and interlayer water molecules. LDHs can be expressed as a general formula of $[(M_{1x}^{z+}M_x'^{y+}(OH)_2)]^{w+}(A^{n-})_{w/n}\cdot mH_2O$, where M^{z+} and M'^{y+} are one or more different metal cations, A^{n-} is interlayer anion. The value of z may be 1 but is most commonly 2, and although y can be 4 it is most commonly 3; the overall metal hydroxide layer charge (w) is determined by $w = z(1-x) + xy - 2$ which is compensated by w/n A^{n-} interlayer anions. The possibility of producing a non-toxic, high aspect 2D structure with a controllable layer thickness gives LDHs the possibility of promising applications in gas and moisture barrier coatings on flexible polymeric films.[23,29] However, due to the strong inter-lamellar hydrogen bonding networks and interlayer electrostatic interactions, the exfoliation/delamination of LDHs remains a big challenge in the field.[29–34] The first successful exfoliation of LDHs was reported using a two-step intercalation/exfoliation process.[30] LDHs were intercalated with organophilic

Chemistry Research Laboratory, Department of Chemistry, 12 Mansfield Road, OX1 3TA, Oxford, UK. E-mail: Dermot.ohare@chem.ox.ac.uk

† Electronic supplementary information (ESI) available: FTIR, PXRD, TGA, BET and TEM. See DOI: 10.1039/d0ma00986e

anions (*e.g.* dodecyl sulfate) followed by delamination in polar organic solvents (*e.g.* alcohols). Hibino and Jones reported another two-step approach in which LDHs were intercalated with amino-carboxylate ions (*e.g.* glycine, serine and L-aspartic acid) and then delaminated in a polar solvent (*e.g.* water, ethanol, acetone, formamide, ethylene glycol and diethyl ether).[35] Formamide has emerged as one of most common polar solvents for exfoliating LDHs due to the strong interactions between its carbonyl and amino functional groups with the LDHs (including both the layer surface, interlayer water molecules and anions).[36] As a result, formamide can disrupt the hydrogen bonding networks and electrostatic interactions between the layers, facilitating the exfoliation and delamination of LDHs. However, the toxic nature of formamide is major concern in terms of food safety and Good Manufacturing Practice (GMP) traceability.[37] There have been a few reports on a one-step direct synthesis of single-layer LDH nanosheets.[29,38–41] To date, the reported processes have several limitations as they require a high temperature/inert atmosphere, ultrasonic or mechanical treatment; in addition, the use of solvents such as butanol and formamide make it almost impossible to deliver "solvent-free" conditions after these treatments. A greener process was reported in 2014 by the exfoliation of LDHs in aqueous NaOH/urea solution.[42] However, this is not suitable for large scale practical use as a low temperature (−10 °C) is required for achieving exfoliation.

In 2019, O'Hare and co-workers reported a new approach for preparing nanoplatelets *via* calcination/reconstruction of LDHs using glycine.[43,44] A gel-like phase was formed after reconstruction in a concentrated aqueous solution of glycine, resulting in the stabilisation of high aspect ratio LDH nanosheets. It was found that the LDH platelet thickness decreased and the diameter increased with increasing reconstruction time.[43] Although a calcination step is necessary for this approach, it is food safe and much more practical than many of the other reported studies[35,38,42,45,46] as it does not require any toxic chemicals, mechanical treatment, or a special atmosphere. Herein, the effect of amino-acid types (size and functional groups) and LDH structures are studied.

To widen the applicability and flexibility of this process further, the effects of different types of amino acids (with non-polar and polar side chains, listed in Table S1, ESI†) and original morphology of the LDHs (rosette shape in Fig. S1 and hexagonal platelet in Fig. S14, ESI†) on their reconstruction are investigated in this study. The nanoplatelets obtained here were used to prepare coating mixtures and applied onto a polymer film substrate. The barrier and optical properties of the coated films were subsequently examined. All LDHs used in this study were $[Mg_{0.8}Al_{0.2}(OH)_2](CO_3)_{0.1}$ (Mg_4Al–CO_3 LDH) and were treated with ethanol using the AMOST process.[47] The AMO-Mg_4Al–CO_3 LDH was calcined at 450 °C for 12 hours to give $Mg_4Al(O)_x$ LDO and then reconstructed back to the LDH using an aqueous solution containing selected amino acids (2.66 mmol) at 80 °C. After 24 hours, the solid was washed with deionised water followed by centrifugation.

LDH nanosheet synthesis

LDH reconstruction using amino acids with nonpolar side chains

A series of amino acids with nonpolar side chain including glycine, β-alanine, β-leucine, β-phenylalanine, β-aminobutyric acid and γ-aminobutyric acid were employed to study their effect on the LDH reconstruction process from $Mg_4Al(O)_x$ LDO. All studies were performed on $Mg_4Al(O)_x$ LDOs derived from the calcination of rosette-shaped LDHs prepared from the co-precipitation method with AMOST treatment (named as Cop-AMO LDHs). The morphology of the Cop-AMO LDHs and the structures of the non-polar amino acids used are shown in Fig. S1 (ESI†). The reconstruction procedure was conducted at 80 °C for 24 hours, using two different systems: (1) in a round bottom flask using oil bath heating (denoted as RC) and (2) in an autoclave hydrothermal reactor (denoted as HT). The samples were defined as Cop-RC-amino acid and Cop-HT-amino acid, respectively. For example, the sample reconstructed in the presence of glycine using the RC system was named as Cop-RC-glycine.

Fig. S2 (ESI†) displays the appearance of the obtained samples after reconstruction. It was observed that most of the samples presented a transparent gelatinous appearance (except for β-phenylalanine). Similar observations were reported for exfoliated LDH-glycine[48] and LDH-NO_3 in formamide.[49] The gel formation can be explained by the swelling behaviour of these LDHs in the presence of zwitterionic compounds such as carboxylates, sulfonates, and amino acids.[50–57] It has been suggested that hydrogen bonding interactions among zwitterionic species and LDHs (layers, the interlayer water molecules and anions) are necessary for the hydration and swelling of LDHs.[51] Hydrogen atoms and nitrogen atoms with lone pairs in amino acids act as hydrogen bond donors (bonding to water molecules) and hydrogen bond acceptors (accepting hydrogen from water molecules), respectively.[51,58] The swelling behaviour represents the incorporation of water in the interlayer space though the hydrogen bonding network.[51] In this study, the position of the amine group was found to have no effect on gel formation, as no difference was observed between the cases that used β- and γ-aminobutyric acid. However, the hydrophobic property of the amino acid was found to be important on gel formation. LDH cannot form gels in the case of β-phenylalanine due to steric hindrance of the phenyl group (hydrophobic) which suppresses hydrogen bonding formation.

Powder X-ray diffraction (XRD) data of the reconstructed LDHs (Fig. S3, ESI†) are typical of conventional LDHs, where no impurity phases are visible with the exception of those reconstructed with β-leucine and β-phenylalanine. The impurity phases in Cop-HT-β-phenylalanine, Cop-HT-β-leucine and Cop-RC-β-phenylalanine arise from the amino acid crystallisation due to their low water solubility (Table S1, ESI†). The interlayer *d*-spacings (003 reflection) are summarised in Table S2 (ESI†). Generally, the *d*-spacing of the reconstructed LDHs (except of Cop-RC-leucine, Cop-HT-leucine and Cop-HT-phenylalanine) are in the range 7.7–7.9 Å which is slightly lower than that of their

pristine Cop-AMO LDHs (7.93 Å) which contains carbonate in the interlayer galleries. The $Mg_4Al(O)_x$ LDO samples reconstructed in the presence of leucine exhibited a larger spacing in the range of 12–13 Å. It was postulated that those molecules, of 9.7 Å in length and 4.7 Å in width,[59] prefer a bilayer arrangement in the LDH interlayers through the oxygen atoms of the carboxylate group, giving a net positive charge on the layer.[60] It is found that the basal spacing was expanded to 15.43 Å in the Cop-HT-β-phenylalanine, indicating that β-phenylalanine was intercalated into the LDH interlayer under hydrothermal reaction at 80 °C.

Fourier transform infrared (FTIR) spectra between 600 and 4000 cm^{-1} were recorded for all samples (Fig. S4, ESI†). All LDH based samples presented a broad band in the region of 3000–3600 cm^{-1}, which is assigned to O–H stretching vibrations due to the hydroxide groups of LDH and water molecules. An absorption at around 1640 cm^{-1} is ascribed to the bending mode of water molecules. The intense carbonate vibration at 1370 cm^{-1} (the υ_3 carbonate stretching mode in D_{3h} symmetry)[61] was observed in Cop-AMO LDHs. However, it is slightly weaker and is overlapped with the symmetric carboxylate vibration band of at 1400 cm^{-1} in all Cop-RC-amino acid and Cop-HT-amino acid samples.

In addition, the asymmetric stretching vibrations of the carboxylate groups at around 1540 cm^{-1} were present in all LDH samples reconstructed in the presence of amino acids, which indicates that amino acids remain in the samples after reconstruction. The weak absorption at 770 cm^{-1} was observed in Cop-RC-β-phenylalanine, due to the mono-substituted benzene.[62]

Transmission electron microscopy (TEM) was used to determine the morphology, particle size and size distribution. As shown in Fig. 1, Fig. S5 and Table S1 (ESI†), all Cop-RC-amino acids presented well dispersed and small platelets after reconstruction using calcined Cop-AMO LDHs with rosette morphology (Fig. S1, ESI†). The size of Cop-RC-amino acids was in the range of 40–181 nm which is much smaller than that of the pristine Cop-AMO LDHs. A similar phenomenon was observed for Cop-HT-amino acid samples. It is believed that hydrogen bonds play an important role in directing the morphology transformation of the LDOs during reconstruction in the presence of amino acids. Newman *et al.* suggested that the oxygen atoms of the carboxylate group in the amino acid can form hydrogen bonds with the hydroxide layers during reconstruction of the LDO into the LDH. Interaction of the layers with unbound amino groups[60] may contribute to the observed increase in the zeta potentials of the LDHs from 12.8 to 32–40 mV after the reconstruction process (Fig. S6, ESI†).

The thermal properties of Cop-AMO LDH, LDO and Cop-RC-amino acids were determined by thermogravimetric analysis (TGA), as shown in Fig. S7 (ESI†). For amino acid reconstructed LDHs, the total mass loss increased with increasing molecular weight of the amino acid, 50 to 60 wt% for glycine and phenylalanine, respectively. Three weight loss events were observed for all amino acid reconstructed LDHs as shown in the differential thermogravimetric (DTG) curves (Fig. S8, ESI†). The first step occurs below 200 °C due to the removal of

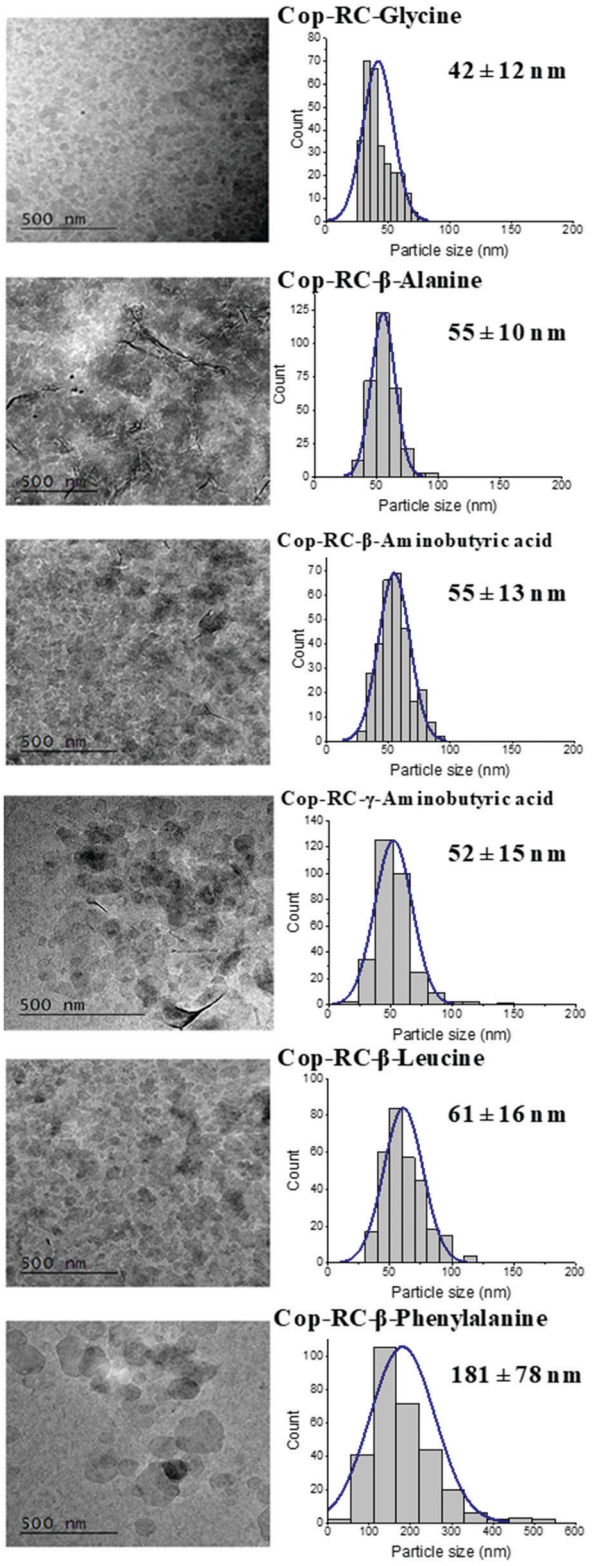

Fig. 1 TEM images and particle size distributions of Cop-RC-amino acids using different nonpolar amino acids. Navy lines indicate the best fit of a Gaussian distribution, showing approximately a normal distribution. Mean values and standard deviations were obtained from the measurement of 300 particles.

adsorbed water and interlayer water. The second step in the range of 250–400 °C is ascribed to the dehydroxylation of the LDH layers and the decomposition of the amino acids and carbonate anions. The last step corresponds to the combustion of the intercalated amino acids and the formation of a carbonaceous residue produced from decomposition of the amino acid.[63] The amino acid content in all reconstructed products was determined by elemental microanalysis (EA), and these results are summarised in Table S4 (ESI†). The EA data indicate a significant reduction of the carbonate anion concentration in the interlayer galleries of the LDH after reconstruction.

LDH reconstruction using amino acids with polar side chains

Amino acids containing different polar side chains: serine (an additional OH group), asparagine (with an additional amide group), aspartic and glutamic acids (an additional carboxylate group) were also used for reconstruction of the LDH. Their structures are presented in Fig. S9 (ESI†). All studies were performed with Cop-AMO LDHs. The reconstruction step was conducted in a round bottom flask at 80 °C for 24 hours. The samples were defined as for the Cop-RC-amino acids (*e.g.* the sample reconstructed in the presence of serine was named Cop-RC-serine).

Gel-like products were obtained in the case of asparagine and serine (Fig. S10, ESI†). Asparagine and serine contain additional amide and hydroxyl functional groups that could participate in the formation of hydrogen bond networks resulting in swelling and gel formation of the LDH nanosheets during reconstruction. However, Cop-RC-serine exhibited a brownish colour, which may be due to a chemical reaction between this amino acid and LDHs during heating (80 °C). In the case of the amino acids with acidic side chains (aspartic and glutamic acids), gel formation was not observed (Fig. S11, ESI†). Although the additional carboxylate group could also form hydrogen bonds, it may preferentially interact with the LDH layers by electrostatic attraction rather than engaging in extensive hydrogen bonding with water and the LDH. In addition, these amino acids are much less soluble in water which may limit the swelling/exfoliation of the LDH platelets, yielding white solid products rather than gel-like LDH suspensions.

Fig. S12 (ESI†) displays the TEM images of the Cop-RC-amino acids using different polar amino acids and Table S5 (ESI†) summaries their particle size distributions. Well-dispersed LDH nanoplatelets were formed after reconstruction in the presence of asparagine or serine with platelet diameters of around 63 and 25 nm, respectively. Cop-RC-glutamic acid showed a mixture of small platelets (59 nm) and some large LDH rosettes (similar to pristine Cop-AMO LDHs). Cop-RC-aspartic acid presented a very different morphology with a flower like shape. The formation of this morphology is still unclear. Fig. S13 (ESI†) shows the XRD data (Fig. S13a, ESI†) and FTIR spectra (Fig. S13b, ESI†) of the reconstructed LDHs in the presence of amino acids with polar side-chains. The interlayer separations of the isolated LDHs are summarised in Table S5 (ESI†), and the values agree with the data reported in the literature using traditional methods; in all cases we noted a small shift in the Bragg peak positions compared with the original parent LDH.[50] The molecular vibrations corresponding the amino acid could be observed in each Cop-RC-amino acid, indicating that the amino acids were present in the reconstructed LDHs.

Effect of original LDHs morphology

To investigate the effect of the original morphology, LDH platelets (prepared using a urea hydrothermal method, UHT-AMO LDHs) were examined with the series of amino acids with nonpolar side chains. The UHT-AMO LDHs have regular hexagonal platelets with the size of 3–4 μm as shown in Fig. S14 (ESI†). These were then was calcined at 450 °C for 12 hours to give the UHT-AMO LDO. The two reconstruction conditions (RC and HT) were also compared at 80 °C for 24 hours, from which the samples were defined as UHT-RC-amino acid and UHT-HT-amino acid, respectively.

Similar to that of Cop-RC-amino acid and Cop-HT-amino acid, gel-like products were observed in most of UHT-RC-amino acids and UHT-HT-amino acids (Fig. S15, ESI†). However, solid products were formed using both leucine and phenylalanine even with hydrothermal conditions, while gel products were obtained in the co-precipitation of LDH with leucine, indicating that the swelling and gel formation behaviour of the LDHs depends on the type of amino acid, the reconstruction conditions and the morphology of the LDHs. The XRD patterns of all samples are shown in Fig. S16 (ESI†) and the *d*-spacing values are summarised in Table 1. No expansion of the layer spacing was observed using small amino acids. An increase of the basal spacing was observed in samples produced from leucine and phenylalanine (12 Å), indicating that the leucine and phenylalanine might be partially intercalated into the LDH interlayer. The FTIR spectrum of all reconstructed LDHs are presented in Fig. S17 (ESI†). The vibration bands for both the asymmetric and symmetric stretch of COO^- and the bending vibration of C–H at 1540, 1400 and 1500 cm^{-1}, respectively, were observed in all UHT-RC-amino acids and UHT-HT-amino acids, suggesting the presence of amino acid molecules in the samples. The carbonate band at 1370 cm^{-1} was observed in all

Table 1 Summary of interlayer spacing of UHT-RC-amino acids and UHT-RC-amino acids

Sample	Interlayer spacing (Å)
UHT-AMO LDHs	7.62
UHT-RC-glycine	7.58
UHT-RC-β-alanine	7.36
UHT-RC-β-aminobutyric acid	7.61
UHT-RC-γ-aminobutyric acid	7.51
UHT-RC-β-leucine	7.65, 12.08
UHT-RC-β-phenylalanine	8.12
UHT-HT-glycine	7.52
UHT-HT-β-alanine	7.6
UHT-HT-β-aminobutyric acid	7.63
UHT-HT-γ-aminobutyric acid	7.56
UHT-HT-β-leucine	7.55, 11.99
UHT-HT-β-phenylalanine	8.08

samples (except for UHT-AMO-LDO) indicating the co-intercalated carbonate ion in the samples.[61]

TEM images and particle size distributions of all UHT-RC-amino acids and UHT-HT-amino acids are shown in Fig. S18 (ESI†) and Fig. 2. The UHT-RC-amino acids present a mixture of small and large particles (Fig. S18, ESI†). The size of the small particles is in the range of 87 ± 22 nm to 352 ± 172 nm whereas the large particle size is the same as that of the pristine UHT-AMO-LDH (3–4 μm). For the UHT-HT-amino acids (Fig. 2), nearly all of the large platelets from pristine UHT-AMO-LDHs were transformed into small particles after hydrothermal treatment in the presence of amino acids. Normally, hydrothermal conditions favour the formation of LDHs with a larger particle size. In this study, the presence of the amino acid was found to play an important role in the transformation of small LDH platelets from large platelets. Generally, the inter-lamellar hydrogen bonding networks and interlayer electrostatic interactions in the LDHs lead to tight stacking among layers and prevent the exfoliation of the LDH layers in water or in solvents.[29–34] These interactions can be weakened by the removal of water during calcination. The reformation of the layer structure depends on the hydration and swelling processes. H-bonds can form immediately once the LDOs are in the amino acid aqueous solution. The amino acid molecules may disrupt the hydrogen bonding networks within the LDH structure and the electrostatic interaction from water and other anions (hydroxide and carbonate), which prevents stacking of the layer and avoids aggregation of the primary particles. On the other hand, the LDOs are undergoing a dissolution–recrystallisation process, which was initially proposed by Stanimirova *et al.*[64–66] The pristine UHT-AMO-LDO large platelets can partially dissolve and recrystallise into small platelets with the help of the amino acid molecules.

Oxygen barrier performance of coated films

The demand for flexible packaging (paper, plastics, and complex/multi-layer materials) is increasing across many industries (*e.g.* food and beverages, cosmetics, and healthcare). High-performance film structures with high barrier properties will soon dominate the market.[67] A concerted effort is now underway to both simplify the film structures and improve the gas barrier performance of the polymeric materials.[68–73] One of the criteria used for selecting the polymer for a coating mixture is its film formation property, which requires that the polymer molecules are mobile and stable during the early stage of solvent evaporation and/or solvent absorption into the substrate.[74] The polymer needs to be solvated to resist precipitation. If precipitation occurs before film formation, a powdery solid will be obtained after drying.[74] Polyvinyl alcohol (PVA) is a water soluble polymer, has good film formation characteristics (ability to form homogeneous films after solvent evaporation), is non-toxic, and has moderate gas barrier properties.[75] Hence, PVA was employed as the polymeric binder in this study.

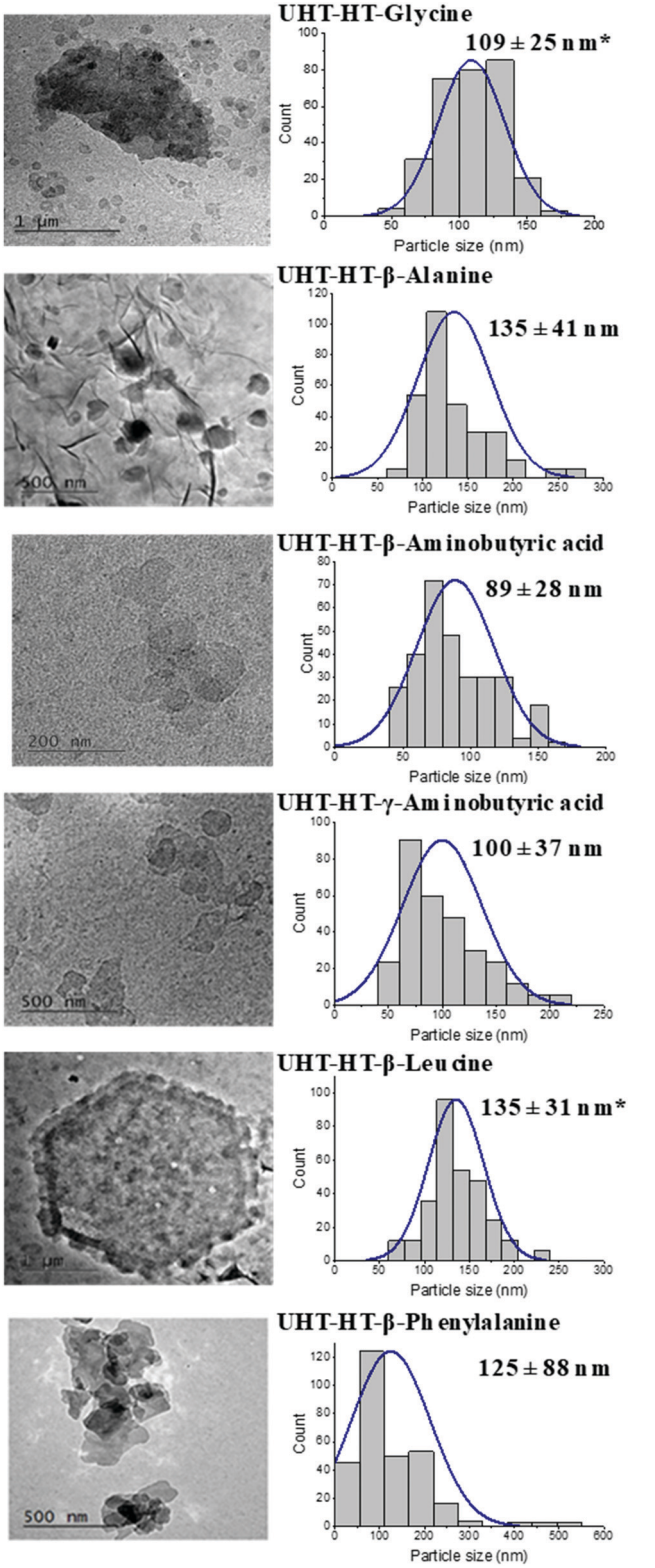

Fig. 2 TEM images with particle size distributions of UHT-HT-amino acids. Navy lines indicate the best fit of a Gaussian distribution, showing approximately a normal distribution. Mean values and standard deviations were obtained from the measurement of 300 particles. '*' indicates that only small sized particles were plotted in the size distribution curves.

Aqueous coating mixtures were prepared by mixing the LDH nanosheets with PVA (Kuraray; Mowiol 4-88, M_w 31 000 g mol^{-1}, 88% hydrolysis) at specific LDHs/PVA weight ratios. The total solid content of the coating formulation was fixed at 5 wt%. The coatings were applied to a corona-treated polyethylene terephthalate (PET) substrate, using an automatic coater, and then dried naturally at room temperature. The PET substrate and the film coated with 5 wt% PVA were prepared and tested as control samples. The effect of the pristine LDH morphology, the LDHs/PVA ratio, the number of coating layers and the types of amino acids are investigated in this study for the barrier performance of the film on the PET substrate.

The oxygen transmission rate (OTR) is a measurement of the rate of oxygen transmission through a film under defined conditions of temperature and relative humidity.[76,77] It is widely accepted that a material can be considered a 'high oxygen barrier' if its OTR is less than 1 cc m^{-2} day^{-1} (at 23 °C, 0% RH).[77,78]

Effect of LDH nanoplatelets on oxygen barrier

In general, the permeation of the polymer filled flake-like particle system depends on the morphology, loading level, coating thickness and orientation of the platelets.[6–8] To study the effect of the pristine LDH morphology, Cop-RC-β-aminobutyric acid (using Cop-AMO LDHs with a rosette shape) and UHT-RC-β-aminobutyric acid (using UHT-AMO LDHs with a platelet shape) were selected for preparing the coating mixtures. Fig. S19 (ESI†) shows the results for the OTR of the PET substrate, the PVA/PET film and the LDHs/PVA/PET films. It was found that a PVA coating alone enhanced the barrier performance of PET with a reduction of the OTR value from 61.30 to 16.30 cc m^{-2} day^{-1}. However, films coated with a mixture of PVA and LDH nanoplatelets (Cop-RC-β-aminobutyric acid and UHT-RC-β-aminobutyric acid) further enhance the oxygen barrier performance by significantly decreasing the OTR to below 6.7 cc m^{-2} day^{-1}. In particular, the Cop-RC-β-aminobutyric acid/PVA/PET film with a Cop-RC-β-aminobutyric acid/PVA ratio of 50/50 exhibited an OTR value as low as 2.85 cc m^{-2} day^{-1}. It is worth noting that the films only contain a single coating layer with a thickness of around 1 μm. This indicates that the incorporation of the designed LDH nanoplatelets in the thin coating layer can efficiently increase the diffusion pathway of the oxygen molecules through the substrate, suggesting that a tortuous pathway has been created even just using a single coating layer.[6,7,79–82] Comparing the different pristine LDH morphologies, the films (Cop-RC-β-aminobutyric acid/PVA/PET from pristine LDH rosettes) presented lower OTR values than those using pristine LDH platelets regardless of the LDHs/PVA ratio. This could be because Cop-RC-β-aminobutyric acid had smaller particles and a better particle uniformity than UHT-RC-β-aminobutyric acid, as shown in Fig. 1 and Fig. S18 (ESI†).

The ratio of LDH nanoplatelets/PVA (with a fixed total solid content of 5 wt%) was investigated for its effect on the barrier performance of the coated films. As shown in Fig. S19 (ESI†), the OTR of the Cop-RC-β-aminobutyric acid/PVA/PET films decreased firstly from 3.17 to 2.85 cc m^{-2} day^{-1} with increasing LDH/PVA ratio from 40/60 to 50/50. However, it increased to 6.70 cc m^{-2} day^{-1} when the LDH/PVA ratio was increased to 70/30. It is possible that too high LDH loading may cause aggregation of the LDH particles, leading to an open structure within the coating layer.[83–85] The UHT-RC-β-aminobutyric acid/PVA/PET films showed the same tendency.

Double coating layers were also studied to investigate the barrier performance. As shown in Fig. 3, the OTR values of all Cop-RC-β-aminobutyric acid/PVA/PET and UHT-RC-β-aminobutyric acid/PVA/PET films were further reduced. In particular, the

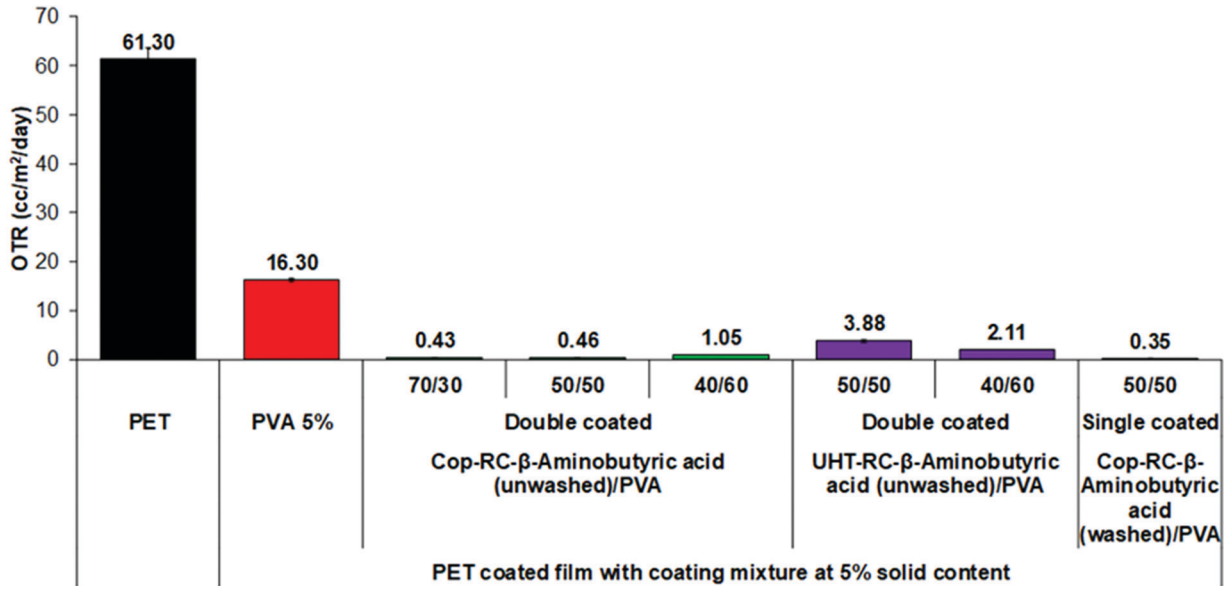

Fig. 3 OTR values of PET, PVA, Cop-RC-β aminobutyric acid/PVA/PET film (green) and UHT-RC-β-aminobutyric acid/PVA/PET (purple) film with a coating mixture at 5 wt% solid content. Double layer coated film with a coating mixture containing unwashed LDHs/PVA at various ratios. Single layer coated film with a coating mixture containing washed Cop-RC-β-aminobutyric acid/PVA at the ratio of 50/50 (blue).

Cop-RC-β-aminobutyric acid/PVA/PET films (with an LDH/PVA ratio of 70/30) showed the lowest OTR value of 0.43 cc m^{-2} day^{-1}. Double coating layers can lead to a thicker coating layer, and a longer diffusing pathway, resulting in a dramatically improved barrier performance even using coatings with a high LDH/PVA ratio.

Both the Cop-RC-β-aminobutyric acid and UHT-RC-β-aminobutyric acid as mentioned above were used directly from the gel after the reconstruction process for coating (*i.e.* without washing). As a result these coatings may contain excess amino acid. Although the OTR may be reduced by adding only amino acids to the PVA coating solution (Fig. S20, ESI†), our study found that the excess amount of amino acid in the reconstructed LDHs had a reverse effect. As shown in Fig. 3, after the removal of excess amino acid, the barrier performance of the Cop-RC-β-aminobutyric acid/PVA/PET film (LDH/PVA ratio of 50/50) significantly improved with the OTR decreasing from 2.85 to 0.35 cc m^{-2} day^{-1}.

Effect of different amino acids

The effect of the different amino acids used in the reconstruction of the Cop-AMO LDHs was examined for their barrier performance. As shown in Fig. S21 (ESI†), the LDH platelets reconstructed in the presence of glycine, alanine or β-aminobutyric acid exhibited a very high oxygen barrier performance, with very low OTR values in the range of 0.35–0.431 cc m^{-2} day^{-1} and an oxygen permeability as low at 0.008 cc mm m^{-2} day^{-1} (Table S6, ESI†). As discussed earlier, the samples (Cop-RC-glycine, Cop-RC-alanine and Cop-RC-β-aminobutyric acid) formed a stable gel phase containing uniform platelets with diameters in the range of 42–55 nm. These platelets can be well dispersed in the coating mixture producing highly aligned nanoplatelets during the film coating process, forming films with a high gas barrier. However, in the cases of β-leucine and β-phenylalanine, their OTR values are 9.6 and 47.65 cc m^{-2} day^{-1}, respectively. This might be due to their non-uniform particle diameters (Fig. 1) and the presence of some crystalline amino acid impurities (Fig. S3, ESI†). We believe the presence of insoluble β-leucine and β-phenylalanine crystals may interfere with the alignment of the LDH nanosheets during the film forming process.

Fig. S22 (ESI†) shows the cross-section SEM images of the coated films with different sized LDHs. All of them show poor dispersion and with aggregation of the LDHs on the coated films, showing the thickness of the coating layer to be in the range of 0.5–1.5 μm, which correlates with the thickness values of the coated films as shown in Fig. S24(a) (ESI†). A high barrier coating will be obtained if the LDH surface is modified to improve the dispersion of the LDHs and their coverage on the substrate. In the case of reconstructed LDHs with amino acid, the coated layer was not clearly resolved by SEM (Fig. S23, ESI†), which may be due to the very thin thickness of the coating layer. No difference in the film thickness was observed between the coated and uncoated film measurements (Fig. S24(b), ESI†).

Optical properties of coated films

The optical properties of the obtained films were evaluated by measuring the total transmittance, clarity and haze.[76] Total transmittance is the ratio of transmitted light to the incident light. The clarity (see-through quality) is determined in an angle range smaller than 2.5°, which describes how well very fine details can be seen through the specimen. The haze measurement is the ratio of transmitted light which, in passing through the specimen, deviates from the incident beam greater than 2.5° on average.

In general, the light scattering of inorganic nanoparticles is responsible for the opacity of composite materials.[86–88] To obtain a highly transparent film, the size of the nanoparticles in the matrix

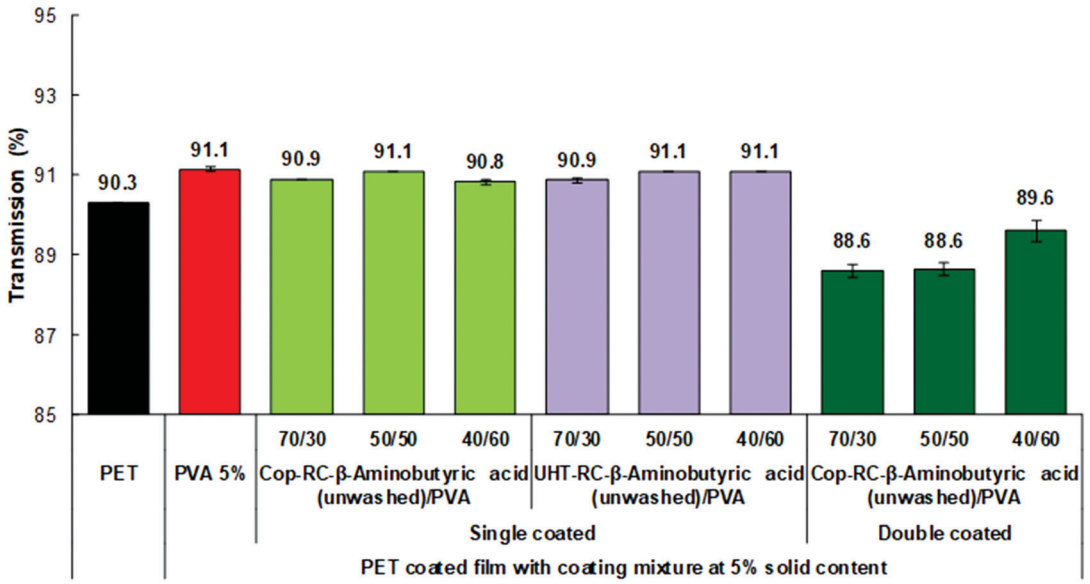

Fig. 4 Optical transmission of the coated films with Cop-RC-β aminobutyric acid at different ratios with a 5 wt% solid content.

should be less than one-tenth of the wavelength of visible light (400–790 nm) to avoid Rayleigh scattering. The lower the Rayleigh scattering, the higher the transparency of the sample.[86–88] As shown in Fig. 4, all Cop-RC-β-aminobutyric acid/PVA/PET and UHT-RC-β-aminobutyric acid/PVA/PET films with a single coating layer present a high transmittance, similar to that of the PET substrate regardless of the LDHs/PVA ratio, indicating that Rayleigh scattering can be avoided by the uniform LDH nanoplatelets with particle diameters mainly in the range of 55–89 nm. Similar results (Fig. S25a, ESI†) were found in the films using LDH nanoplatelets reconstructed in the presence of other nonpolar amino acids (such as glycine, β-alanine, β-leucine, β-phenylalanine and γ-aminobutyric acid). However, if a second coating layer is applied, the transparency of the Cop-RC-β-aminobutyric acid/PVA/PET film with a higher LDHs/PVA ratio decreased from 90.3 to 88.6%. The thicker coating layer with a higher LDH nanoplatelet loading can increase the light scattering, leading to a lower transparency. The clarity depends on the size distribution of the particles: a narrow particle size distribution yields a coated film with a high film clarity.[89] As shown in Fig. S26a (ESI†), the Cop-RC-β-aminobutyric acid/PVA/PET and UHT-RC-β-aminobutyric acid/PVA/PET films show a clarity similar to that of the PET substrate regardless of the coating layers (Fig. 4). Similar findings were observed (Fig. S25b, ESI†) for films using LDH nanoplatelets reconstructed in the presence of other amino acids (*e.g.* glycine, β-alanine, β-leucine and β-phenylalanine and γ-aminobutyric acid). Correspondingly, the haze values of all the LDH/PVA coated films (Fig. S25c and S26b, ESI†) were low, similar to that of the PET substrate with the exception of the ones with higher LDHs/PVA ratios.

Conclusions

The synthesis and characterisation of well-dispersed uniform LDH nanoplatelets *via* a reconstruction process in a concentrated aqueous solution of amino acids was reported. Dispersions of these LDH nanoplatelets in PVA were used to coat PET films for potential application as a non-toxic food packaging material. After amino acid reconstruction, the LDH consists of nanoplatelets and forms a stable transparent gel. The highest propensity for hydrogen bonding facilitates gel formation containing uniform, 40–50 nm diameter, LDH nanoplatelets. These nanoplatelets are an excellent inorganic additive in the PVA. They combine to produce a coating dispersion for deposition on the PET film to provide a high oxygen barrier and good transparency film. The Cop-RC-β-aminobutyric acid (washed)/PVA/PET film exhibited the lowest OTR value of 0.35 cc m^{-2} day^{-1} after a single coating. Single coated LDHs/PVA/PET films retained the excellent optical performance (transmittance, clarity and haze) of the uncoated PET film.

This work provides a facile and cost-effective strategy for the preparation of LDH-based oxygen barrier coated films that could be particularly useful in packaging applications. The non-toxic nature of LDH will potentially allow this system to be applied for food packaging use.

Conflicts of interest

There are no conflicts to declare.

Acknowledgements

K. R. thanks SCG Packaging PLC (Thailand) and C. C., J. Y. and J.-C. B. thank SCG Chemicals Co., Ltd (Thailand) for funding. The authors thank the Product and Technology Development Center (PTDC), SCG Packaging PLC, Ratchaburi for optical testing.

Notes and references

1 N. Farmer, *Trends in Packaging of Food, Beverages and Other Fast-Moving Consumer Goods (FMCG)*, Woodhead Publishing, 2013, pp. 1–21.
2 P. E. Burrows, G. L. Graff, M. E. Gross, P. M. Martin, M. K. Shi, M. Hall, E. Mast, C. Bonham, W. Bennett and M. B. Sullivan, *Displays*, 2001, **22**, 65–69.
3 R. S. Kumar, M. Auch, E. Ou, G. Ewald and C. S. Jin, *Thin Solid Films*, 2002, **417**, 120–126.
4 M. A. Osman, V. Mittal and H. R. Lusti, *Macromol. Rapid Commun.*, 2004, **25**, 1145–1149.
5 Y. Dou, S. Xu, X. Liu, J. Han, H. Yan, M. Wei, D. G. Evans and X. Duan, *Adv. Funct. Mater.*, 2014, **24**, 514–521.
6 L. E. Nielsen, *J. Macromol. Sci., Part A: Pure Appl. Chem.*, 1967, **1**, 929–942.
7 M. W. Möller, T. Lunkenbein, H. Kalo, M. Schieder, D. A. Kunz and J. Breu, *Adv. Mater.*, 2010, **22**, 5245–5249.
8 T. Ebina and F. Mizukami, *Adv. Mater.*, 2007, **19**, 2450–2453.
9 Z. Tang, N. A. Kotov, S. Magonov and B. Ozturk, *Nat. Mater.*, 2003, **2**, 413–418.
10 I. A. Aksay, M. Trau, S. Manne, I. Honma, N. Yao, L. Zhou, P. Fenter, P. M. Eisenberger and S. M. Gruner, *Science*, 1996, **273**, 892.
11 K. S. Aneja, H. L. M. Böhm, A. S. Khanna and S. Böhm, *FlatChem*, 2017, **1**, 11–19.
12 Y. Cui, S. I. Kundalwal and S. Kumar, *Carbon*, 2016, **98**, 313–333.
13 Y. Hernandez, V. Nicolosi, M. Lotya, F. M. Blighe, Z. Sun, S. De, I. T. McGovern, B. Holland, M. Byrne, Y. K. Gun'Ko, J. J. Boland, P. Niraj, G. Duesberg, S. Krishnamurthy, R. Goodhue, J. Hutchison, V. Scardaci, A. C. Ferrari and J. N. Coleman, *Nat. Nanotechnol.*, 2008, **3**, 563–568.
14 M. Lotya, Y. Hernandez, P. J. King, R. J. Smith, V. Nicolosi, L. S. Karlsson, F. M. Blighe, S. De, Z. Wang, I. T. McGovern, G. S. Duesberg and J. N. Coleman, *J. Am. Ceram. Soc.*, 2009, **131**, 3611–3620.
15 U. Khan, A. O'Neill, M. Lotya, S. De and J. N. Coleman, *Small*, 2010, **6**, 864–871.
16 S. Vadukumpully, J. Paul and S. Valiyaveettil, *Carbon*, 2009, **47**, 3288–3294.
17 Y. Chen, G. Yang, Z. Zhang, X. Yang, W. Hou and J.-J. Zhu, *Nanoscale*, 2010, **2**, 2131–2138.

18 A. V. Murugan, A. K. Viswanath, C. S. Gopinath and K. Vijayamohanan, *J. Appl. Phys.*, 2006, **100**, 074319.
19 G. Alberti, C. Dionigi, E. Giontella, S. Murcia-Mascarós and R. Vivani, *J. Colloid Interface Sci.*, 1997, **188**, 27–31.
20 L. Sun, W. J. Boo, D. Sun, A. Clearfield and H.-J. Sue, *Chem. Mater.*, 2007, **19**, 1749–1754.
21 P. F. Luckham and S. Rossi, *Adv. Colloid Interface Sci.*, 1999, **82**, 43–92.
22 Y. Cui, S. Kumar, B. Rao Kona and D. van Houcke, *RSC Adv.*, 2015, **5**, 63669–63690.
23 W. Hou, L. Kang, R. Sun and Z.-H. Liu, *Colloids Surf., A*, 2008, **312**, 92–98.
24 Z. Liu, R. Ma, M. Osada, N. Iyi, Y. Ebina, K. Takada and T. Sasaki, *J. Am. Ceram. Soc.*, 2006, **128**, 4872–4880.
25 F. Leroux and J. P. Besse, *Chem. Mater.*, 2001, **13**, 3507–3515.
26 Z. h. Liu, X. Yang, Y. Makita and K. Ooi, *Chem. Mater.*, 2002, **14**, 4800–4806.
27 J. Miao, M. Xue, H. Itoh and Q. Feng, *J. Mater. Chem.*, 2006, **16**, 474–480.
28 M. Yoonessi, H. Toghiani, T. L. Daulton, J.-S. Lin and C. U. Pittman, *Macromolecules*, 2005, **38**, 818–831.
29 J. Yu, Q. Wang, D. O'Hare and L. Sun, *Chem. Soc. Rev.*, 2017, **46**, 5950–5974.
30 M. Adachi Pagano, C. Forano and J. P. Besse, *Chem. Commun.*, 2000, 91–92.
31 M. Jobbágy and N. Iyi, *J. Phys. Chem. C*, 2010, **114**, 18153–18158.
32 R. Ma and T. Sasaki, *Adv. Mater.*, 2010, **22**, 5082–5104.
33 Q. Wang and D. O'Hare, *Chem. Rev.*, 2012, **112**, 4124–4155.
34 N. Mao, C. H. Zhou, D. S. Tong, W. H. Yu and C. X. Cynthia Lin, *Appl. Clay Sci.*, 2017, **144**, 60–78.
35 T. Hibino and W. Jones, *J. Mater. Chem.*, 2001, **11**, 1321–1323.
36 R. Ma, Z. Liu, L. Li, N. Iyi and T. Sasaki, *J. Mater. Chem.*, 2006, **16**, 3809–3813.
37 EFSA Panel on Additives and Products or Substances used in Animal Feed, *EFSA J.*, 2015, **13**, 4056.
38 J. Yu, B. R. Martin, A. Clearfield, Z. Luo and L. Sun, *Nanoscale*, 2015, **7**, 9448–9451.
39 J. Yu, J. Liu, A. Clearfield, J. E. Sims, M. T. Speiegle, S. L. Suib and L. Sun, *Inorg. Chem.*, 2016, **55**, 12036–12041.
40 T. B. Hur, T. X. Phuoc and M. K. Chyu, *J. Appl. Phys.*, 2010, **108**, 114312.
41 G. Hu, N. Wang, D. O'Hare and J. Davis, *Chem. Commun.*, 2006, 287–289.
42 Y. Wei, F. Li and L. Liu, *RSC Adv.*, 2014, **4**, 18044–18051.
43 J. Yu, K. Ruengkajorn, D.-G. Crivoi, C. Chen, J.-C. Buffet and D. O'Hare, *Nat. Commun.*, 2019, **10**, 2398.
44 J. Yu, J.-C. Buffet and D. O'Hare, *ACS Appl. Mater. Interfaces*, 2020, **12**, 10973–10982.
45 T. Hibino, *Chem. Mater.*, 2004, **16**, 5482–5488.
46 T. Hibino and M. Kobayashi, *J. Mater. Chem.*, 2005, **15**, 653–656.
47 C. Chen, M. Yang, Q. Wang, J.-C. Buffet and D. O'Hare, *J. Mater. Chem. A*, 2014, **2**, 15102–15110.
48 Q. Wu, A. O. Sjastad, O. B. Vistad, K. D. Knudsen, J. Roots, J. S. Pedersen and P. Norby, *J. Mater. Chem.*, 2007, **17**, 965–971.
49 Q. Wu, A. Olafsen, O. B. Vistad, J. Roots and P. Norby, *J. Mater. Chem.*, 2005, **15**, 4695–4700.
50 H. Nakayama, N. Wada and M. Tsuhako, *Int. J. Pharm.*, 2004, **269**, 469–478.
51 N. Iyi, S. Ishihara, Y. Kaneko and H. Yamada, *Langmuir*, 2013, **29**, 2562–2571.
52 S. Aisawa, S. Takahashi, W. Ogasawara, Y. Umetsu and E. Narita, *J. Solid State Chem.*, 2001, **162**, 52–62.
53 N. Iyi, Y. Ebina and T. Sasaki, *J. Mater. Chem.*, 2011, **21**, 8085–8095.
54 N. Iyi, Y. Ebina and T. Sasaki, *Langmuir*, 2008, **24**, 5591–5598.
55 S. Aisawa, S. Sasaki, S. Takahashi, H. Hirahara, H. Nakayama and E. Narita, *J. Phys. Chem. Solids*, 2006, **67**, 920–925.
56 R. Pethig, *IEEE Trans. Electr. Insul.*, 1984, **EI-19**, 453–474.
57 W. M. Arnold and U. Zimmermann, *Biochem. Soc. Trans.*, 1993, **21**, 475S.
58 M. Onikata, M. Kondo and S. Yamanaka, *Clays Clay Miner.*, 1999, **47**, 678.
59 C. B. Ching, K. Hidajat and M. S. Uddin, *Sep. Sci. Technol.*, 1989, **24**, 581–597.
60 S. P. Newman, T. Di Cristina, P. V. Coveney and W. Jones, *Langmuir*, 2002, **18**, 2933–2939.
61 M. J. Hernandez-Moreno, M. A. Ulibarri, J. L. Rendon and C. J. Serna, *Phys. Chem. Miner.*, 1985, **12**, 34–38.
62 M. S. San Román and M. J. Holgado, *Open J. Inorg. Chem.*, 2015, **5**, 52.
63 G. Choi, J.-H. Yang, G.-Y. Park, A. Vinu, A. Elzatahry, C. H. Yo and J.-H. Choy, *Eur. J. Inorg. Chem.*, 2015, 925–930.
64 T. Stanimirova, G. Kirov and E. Dinolova, *J. Mater. Sci. Lett.*, 2001, **20**, 453–455.
65 T. Stanimirova and G. Kirov, *Appl. Clay Sci.*, 2003, **22**, 295–301.
66 T. Stanimirova and V. Balek, *J. Therm. Anal. Calorim.*, 2008, **94**, 477–481.
67 N. Farmer, A. Emblem, J. Plimmer, T. A. Cooper, D. A. Abramowicz, L. Jenkins, B. Fields, K. Ambrose, I. Bucklow, T. Benge, G. Hughes, A. Noke, J. Bilko, A. Ioannides, C. Ramsey, R. Coles, G. Richard Inns, B. Park and P. Butler, *Trends in Packaging of Food, Beverages and Other Fast-Moving Consumer Goods (FMCG)*, Woodhead Publishing, 2013, pp. xi–xii, DOI: 10.1016/B978-0-85709-503-9.50014-X.
68 N. Inagaki, S. Tasaka and H. Hiramatsu, *J. Appl. Polym. Sci.*, 1999, **71**, 2091–2100.
69 K. S. Triantafyllidis, P. C. LeBaron, I. Park and T. J. Pinnavaia, *Chem. Mater.*, 2006, **18**, 4393–4398.
70 M. A. Priolo, D. Gamboa, K. M. Holder and J. C. Grunlan, *Nano Lett.*, 2010, **10**, 4970–4974.
71 M. W. Möller, D. A. Kunz, T. Lunkenbein, S. Sommer, A. Nennemann and J. Breu, *Adv. Mater.*, 2012, **24**, 2142–2147.
72 C. N. Wu, T. Saito, S. Fujisawa, H. Fukuzumi and A. Isogai, *Biomacromolecules*, 2012, **13**, 1927–1932.
73 S. Ming, G. Chen, J. He, Y. Kuang, Y. Liu, R. Tao, H. Ning, P. Zhu, Y. Liu and Z. Fang, *Langmuir*, 2017, **33**, 8455–8462.

74 L. W. Beatty and I. Penboss, *Surface Coatings: Volume 1 Raw Materials and Their Usage*, Springer Netherlands, Dordrecht, 1993, pp. 325–331.
75 H. C. Langowski, *Plastic Packaging*, Wiley-VCH Verlag GmbH & Co. KGaA, 2008, pp. 297–347.
76 B. A. Morris, *The Science and Technology of Flexible Packaging: Multilayer Films from Resin and Process to End Use, Matthew Deans*, Elsevier, Oxford, United Kingdom, 2016.
77 Standard Testing Methods for Flexible Films, http://marketing.sourcebookmaterials.com/hubfs/Resources/White%20Paper%20(Standard%20Testing%20Methods%20for%20Flexible%20Films).pdf, (accessed 09 October 2017, 2017).
78 Oxygen Transmission Rate, http://www.polyprint.com/flexographic-otr.htm, (accessed 09 October 2017, 2017).
79 T. Pan, S. Xu, Y. Dou, X. Liu, Z. Li, J. Han, H. Yan and M. Wei, *J. Mater. Chem. A*, 2015, **3**, 12350–12356.
80 Q. Sun, F. J. Schork and Y. Deng, *Compos. Sci. Technol.*, 2007, **67**, 1823–1829.
81 S. Thomas, A. P. Meera and H. J. Maria, Enhancing Gas-Barrier Properties of Polymer-Clay Nanocomposites, http://www.4spepro.org/view.php?article=004266-2012-07-28&category=Composites, (accessed 08 October 2017, 2017).
82 H. D. Huang, P. G. Ren, J. Chen, W. Q. Zhang, X. Ji and Z. M. Li, *J. Membrane Sci.*, 2012, **409**, 156–163.
83 C. Andersson, *Packag. Technol. Sci.*, 2008, **21**, 339–373.
84 D. R. Paul and L. M. Robeson, *Polymer*, 2008, **49**, 3187–3204.
85 Å. Nyflött, Doctoral Degree Licentiate Thesis, Karlstad University, 2014.
86 H. I. Elim, B. Cai, Y. Kurata, O. Sugihara, T. Kaino, T. Adschiri, A.-L. Chu and N. Kambe, *J. Phys. Chem. B*, 2009, **113**, 10143–10148.
87 T. Itoh, T. Uchida, N. Izu, I. Matsubara and W. Shin, *Materials*, 2013, **6**, 2119–2129.
88 F. Bertrand, S. A. German, A. Anwar, V. Irune, B. Gemma, R. D. M. Yolanda and B. Lennart, *Sci. Technol. Adv. Mater.*, 2013, **14**, 023001.
89 Z. W. Wicks, F. N. Jones, S. P. Pappas and D. A. Wicks, *Organic Coatings: Science and Technology*, Wiley, New Jersey, United States, 2007.